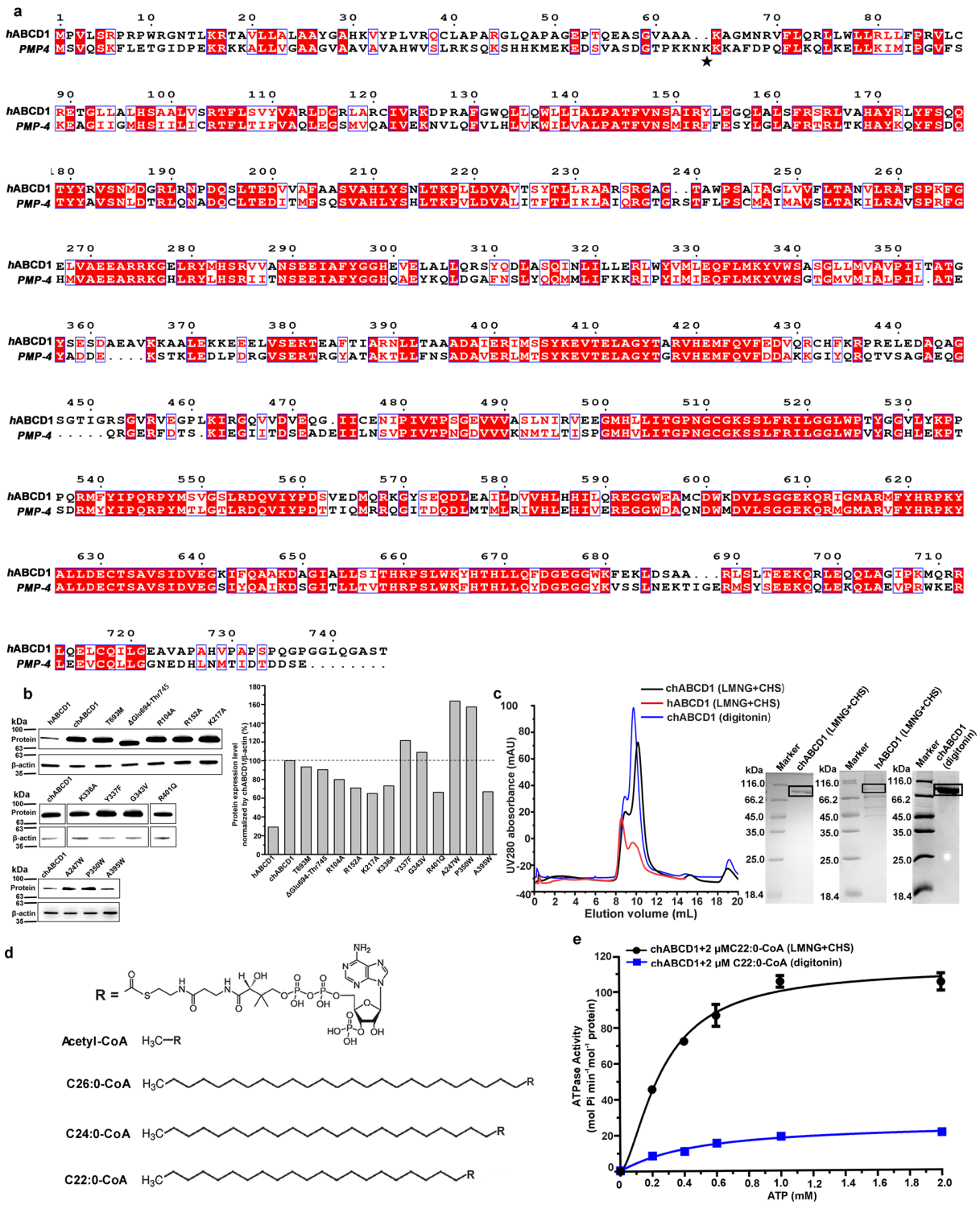


**Supplementary Fig. 1 Construction and purification of ABCD1. a,** Multiple-sequence alignment of human ABCD1 and *Caenorhabditis elegans* PMP-4. A chimeric version of ABCD1

was constructed by replacing the N-terminal 63 residues with the N-terminal 65 residues of PMP-4 The N-terminal Lys65 of PMP-4 is indicated by an asterisk. **b,** The Western blot analysis to quantify the expression levels of the variants in the total cell extracts, β-actin served as an internal control (n=1). The immunoblot of hABCD1, chABCD1 and mutants of chABCD1 were completed in three different experiments, and controls of β-actin and chABCD1 were run on each blot, and the PVDF membranes were sliced into stripes according to a pre-stained protein marker. The expression levels were shown in the bar chart normalized by chABCD1/β-actin (%). The Western blot analysis results is a representatives (n=1) of many times optimized experiments. Source data are provided as a Source Data file. **c.** Representative size-exclusion chromatography profiles and SDS-PAGE analysis of chimeric ABCD1 (chABCD1) and human ABCD1 (hABCD1) using a Superdex 200 increase 10/300 GL SEC column. The peak fractions around 10 mL for human ABCD1 and 10.2 mL for chimeric ABCD1 were pooled and concentrated for biochemical and structural studies. The purified protein was visualized by Coomassie-blue stained SDS-PAGE and bands for chimeric ABCD1 and human ABCD1 were indicated by black rectangles. The chromatogram and SDS-PAGE are representatives of > 5 independent experiments that showed similar results. **d,** Structural formulas of compounds used in the ATPase activity assays. **e,** Substrate concentration-dependent ATPase activity of chABCD1 upon addition of C22:0-CoA in detergent of digitonin or LMNG+CHS. The data points were fitted with a Michaelis-Menten equation. All data points represent means of three independent measurements (n=3). Error bars indicate standard deviation.

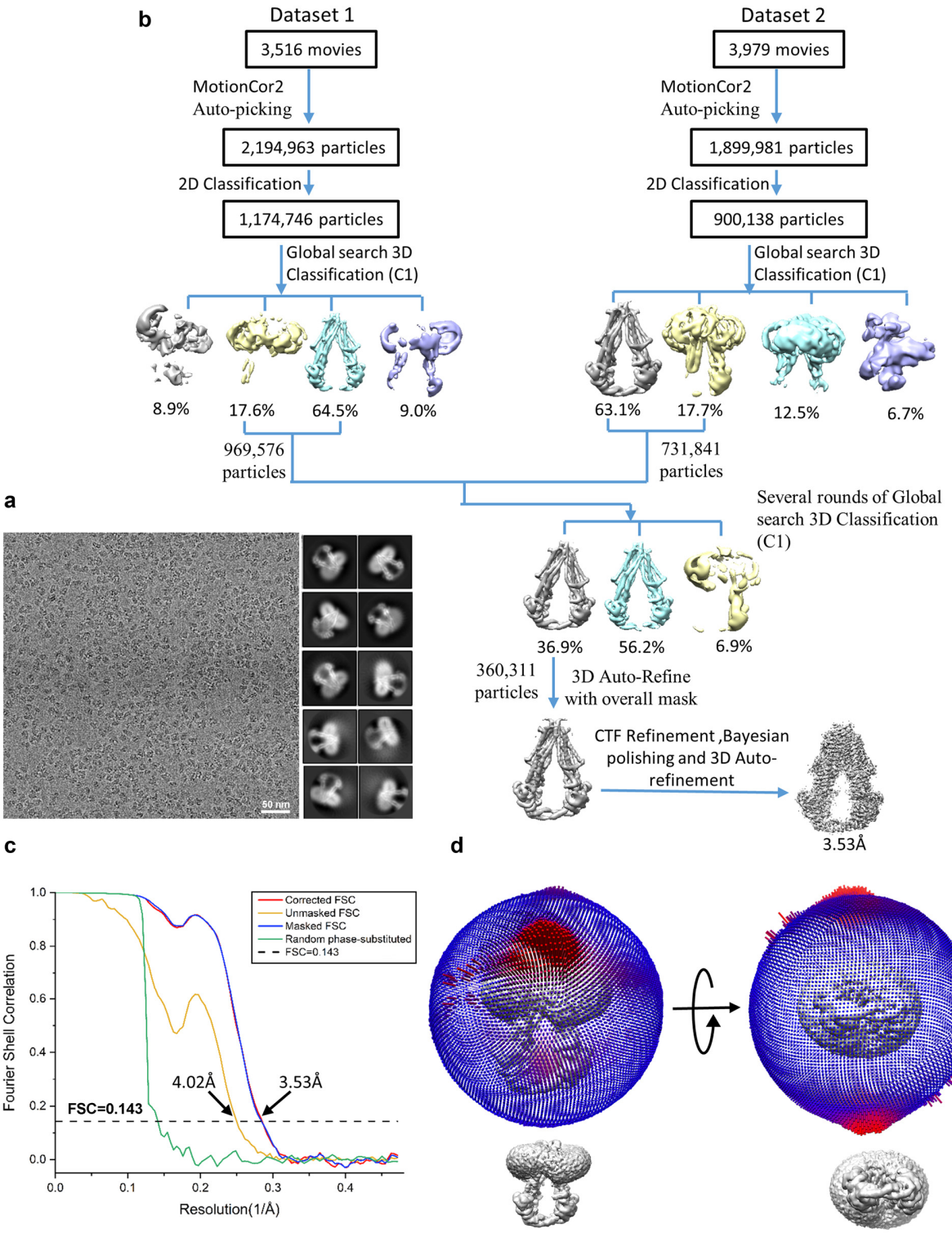
b
Dataset 1
3,516 movies
MotionCor2
Auto-picking
2,194,963 particles
2D Classification
1,174,746 particles
Global search 3D
Classification (C1)
8.9%
17.6%
64.5%
9.0%
969,576
particles
Dataset 2
3,979 movies
MotionCor2
Auto-picking
1,899,981 particles
2D Classification
900,138 particles
Global search 3D
Classification (C1)
63.1%
17.7%
12.5%
6.7%
731,841
particles
Several rounds of Global
search 3D Classification
(C1)
36.9%
56.2%
6.9%
360,311
particles
3D Auto-Refine
with overall mask
CTF Refinement ,Bayesian
polishing and 3D Auto-
refinement
3.53Å
a
50 nm
c
Corrected FSC
Unmasked FSC
Masked FSC
Random phase-substituted
FSC=0.143
Fourier Shell Correlation
4.02Å
3.53Å
FSC=0.143
Resolution(1/Å)
d

25

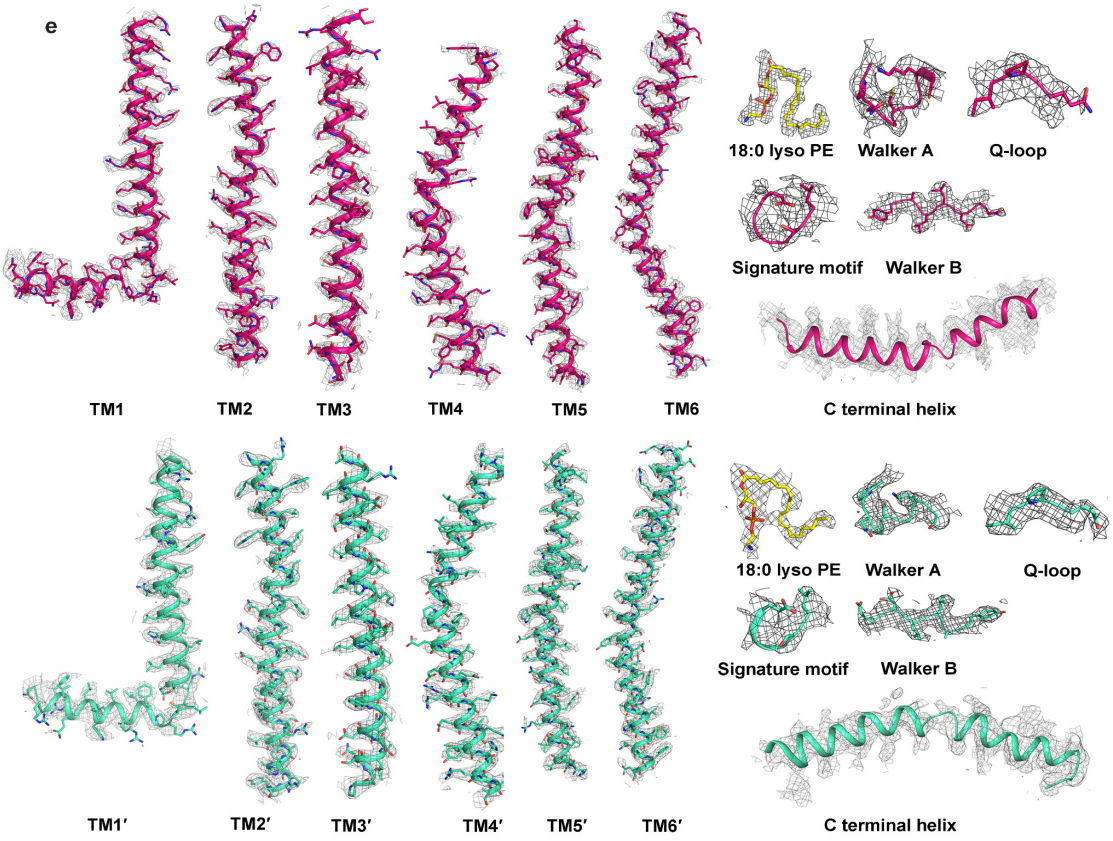


26

27 **Supplementary Fig. 2 Data processing and model building of apo-form ABCD1. a,**
28 Representative cryo-EM micrographs and 2D averages. Bar: 50 nm. The micrograph is a
29 representative of 7,459 cryo-EM images. **b,** Flowchart for cryo-EM data processing. **c,** Gold-
30 standard FSC curve for apo-form ABCD1 map generated using RELION 3.1. **d,** Euler angle
31 distribution of the classified particles used for the final 3D refinement of the overall map. **e,** cryo-
32 EM maps for representative segments of apo-form ABCD1. The structure was reconstructed with
33 C1 symmetry, so all the representative segments in two subunits are thus presented. Contour levels
34 are set at 5σ for TM1-6 and two phosphatidyl ethanolamine (PE) molecules, and at 4σ for the
35 consensus motif in NBDs including Walker A, Q-loop, signature motif, and Walker B. The contour
36 level for C-terminal helix is set at 3σ.

37

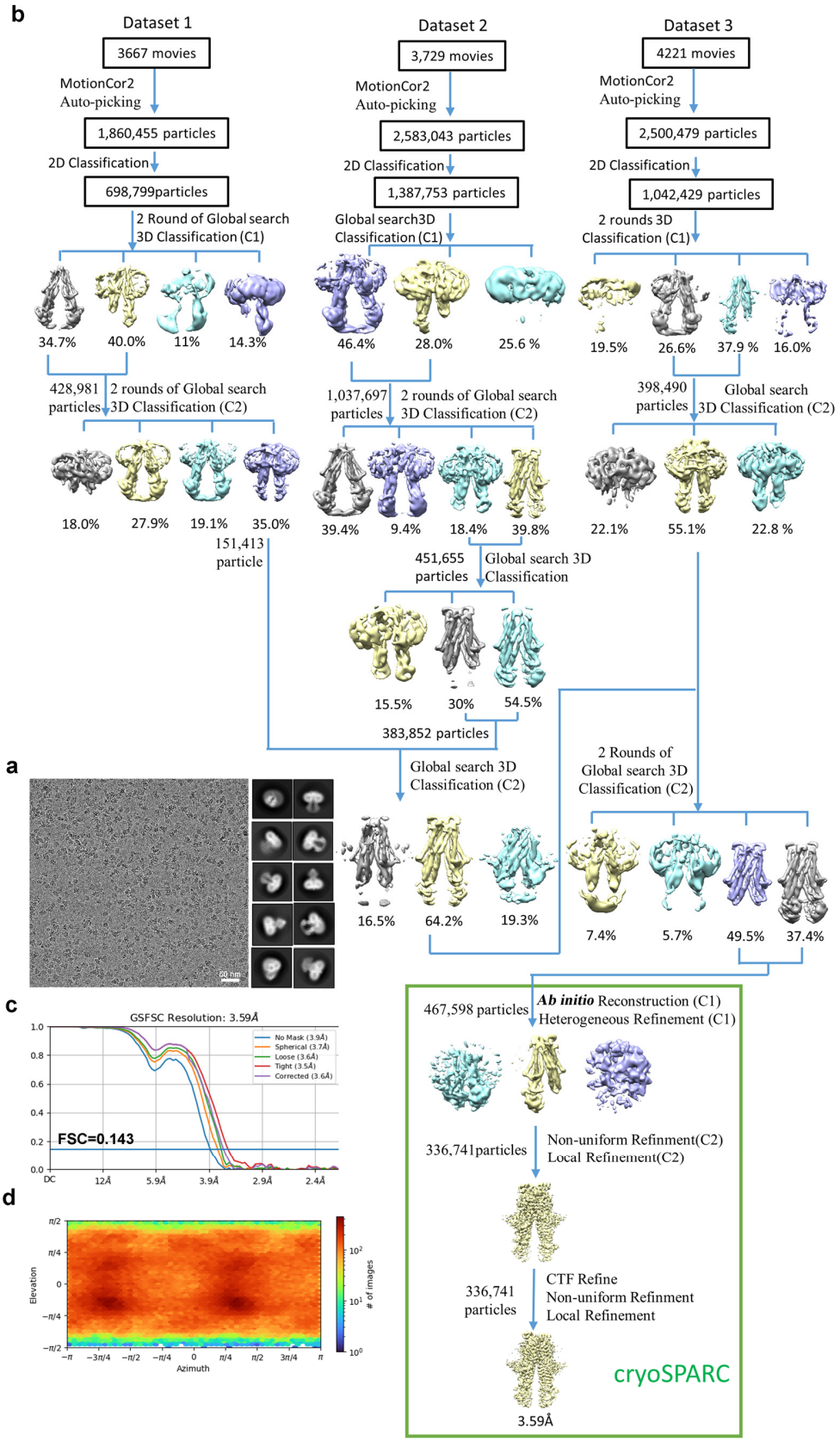
b
Dataset 1
3667 movies
MotionCor2
Auto-picking
1,860,455 particles
2D Classification
698,799particles
2 Round of Global search
3D Classification (C1)
34.7%
40.0%
11%
14.3%
428,981
particles
2 rounds of Global search
3D Classification (C2)
18.0%
27.9%
19.1%
35.0%
151,413
particle
Dataset 2
3,729 movies
MotionCor2
Auto-picking
2,583,043 particles
2D Classification
1,387,753 particles
Global search3D
Classification (C1)
46.4%
28.0%
25.6 %
1,037,697
particles
2 rounds of Global search
3D Classification (C2)
39.4%
9.4%
18.4%
39.8%
451,655
particles
Global search 3D
Classification
15.5%
30%
54.5%
383,852 particles
Global search 3D
Classification (C2)
16.5%
64.2%
19.3%
Dataset 3
4221 movies
MotionCor2
Auto-picking
2,500,479 particles
2D Classification
1,042,429 particles
2 rounds 3D
Classification (C1)
19.5%
26.6%
37.9 %
16.0%
398,490
particles
Global search
3D Classification (C2)
22.1%
55.1%
22.8 %
2 Rounds of
Global search 3D
Classification (C2)
7.4%
5.7%
49.5%
37.4%
a
60 nm
c
GSFSC Resolution: 3.59Å
No Mask (3.9Å)
Spherical (3.7Å)
Loose (3.6Å)
Tight (3.5Å)
Corrected (3.6Å)
FSC=0.143
DC
12Å
5.9Å
3.9Å
2.9Å
2.4Å
d
Elevation
Azimuth
# of images
467,598 particles
Ab initio Reconstruction (C1)
Heterogeneous Refinement (C1)
336,741particles
Non-uniform Refinment(C2)
Local Refinement(C2)
336,741
particles
CTF Refine
Non-uniform Refinment
Local Refinement
3.59Å
cryoSPARC

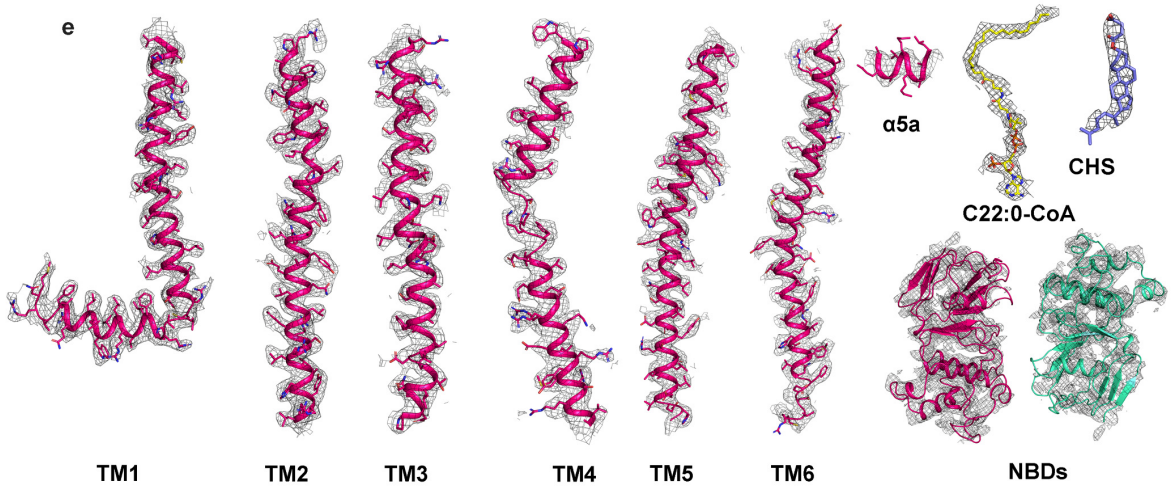


**Supplementary Fig. 3 Data processing and model building of C22:0-CoA-bound ABCD1. a,** Representative cryo-EM micrographs and 2D averages. Bar: 50 nm. The micrograph is a representative of 11,617 cryo-EM images. **b,** Flowchart for cryo-EM data processing. **c,** Gold-standard FSC curve for C22:0-CoA-bound ABCD1 map generated using cryoSPARC 3.1. **d,** Euler angle distribution of the classified particles used for the final 3D refinement of the overall map. **e,** Cryo-EM densities of representative segments of the structure of C22:0-CoA-bound ABCD1. The structure was reconstructed with C2 symmetry, and only one subunit presented. Contour levels are set at 5σ for TM1-6, C22:0-CoA, and at 4σ for CHS. The contour level for the NBDs is set at 3.5σ.

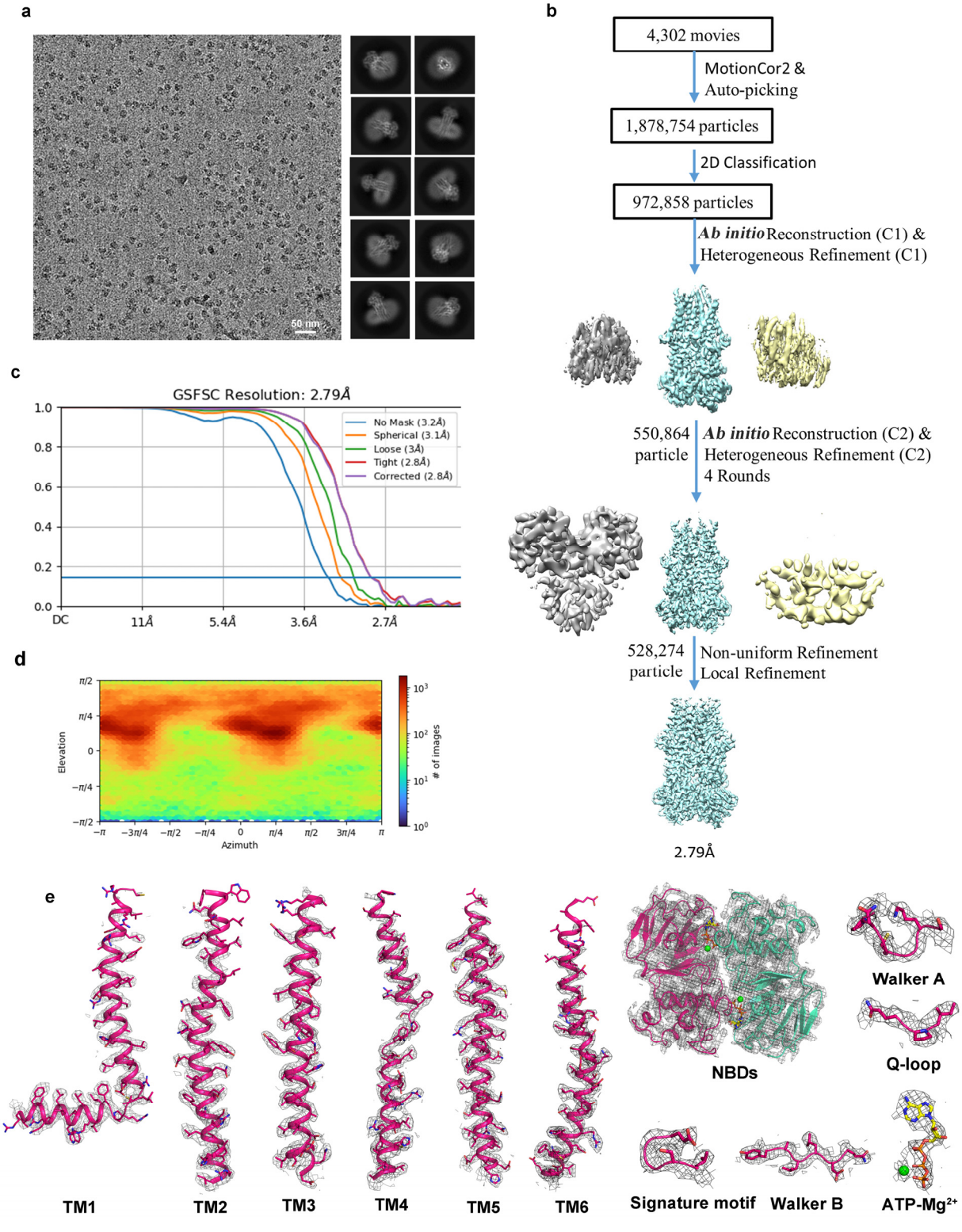
a
50 nm
b
4,302 movies
MotionCor2 &
Auto-picking
1,878,754 particles
2D Classification
972,858 particles
Ab initio Reconstruction (C1) &
Heterogeneous Refinement (C1)
550,864
particle
Ab initio Reconstruction (C2) &
Heterogeneous Refinement (C2)
4 Rounds
528,274
particle
Non-uniform Refinement
Local Refinement
2.79Å
c
GSFSC Resolution: 2.79Å
No Mask (3.2Å)
Spherical (3.1Å)
Loose (3Å)
Tight (2.8Å)
Corrected (2.8Å)
1.0
0.8
0.6
0.4
0.2
0.0
DC
11Å
5.4Å
3.6Å
2.7Å
d
Elevation
Azimuth
# of images
e
TM1
TM2
TM3
TM4
TM5
TM6
NBDs
Walker A
Q-loop
Signature motif
Walker B
ATP-Mg2+

**Supplementary Fig. 4 Data processing and model building of ATP-bound ABCD1. a,** Representative cryo-EM micrographs and 2D averages. Bar: 50 nm. The micrograph is a representative of 4,302 cryo-EM images. **b,** Flowchart for cryo-EM data processing. **c,** Gold-standard FSC curve for ATP-bound ABCD1 map generated using cryoSPARC 3.1. **d,** Euler angle distribution of the classified particles used for the final 3D refinement of the overall map. **e,** Cryo-EM maps for representative segments of ATP-bound ABCD1. The structure was imposed with C2 symmetry, so only segments in one subunit are presented. Contour levels are set at 5σ for TM1-6, NBDs, ATP-$Mg^{2+}$ molecules and the consensus motif in NBDs including Walker A, Q-loop, signature motif, and Walker B.

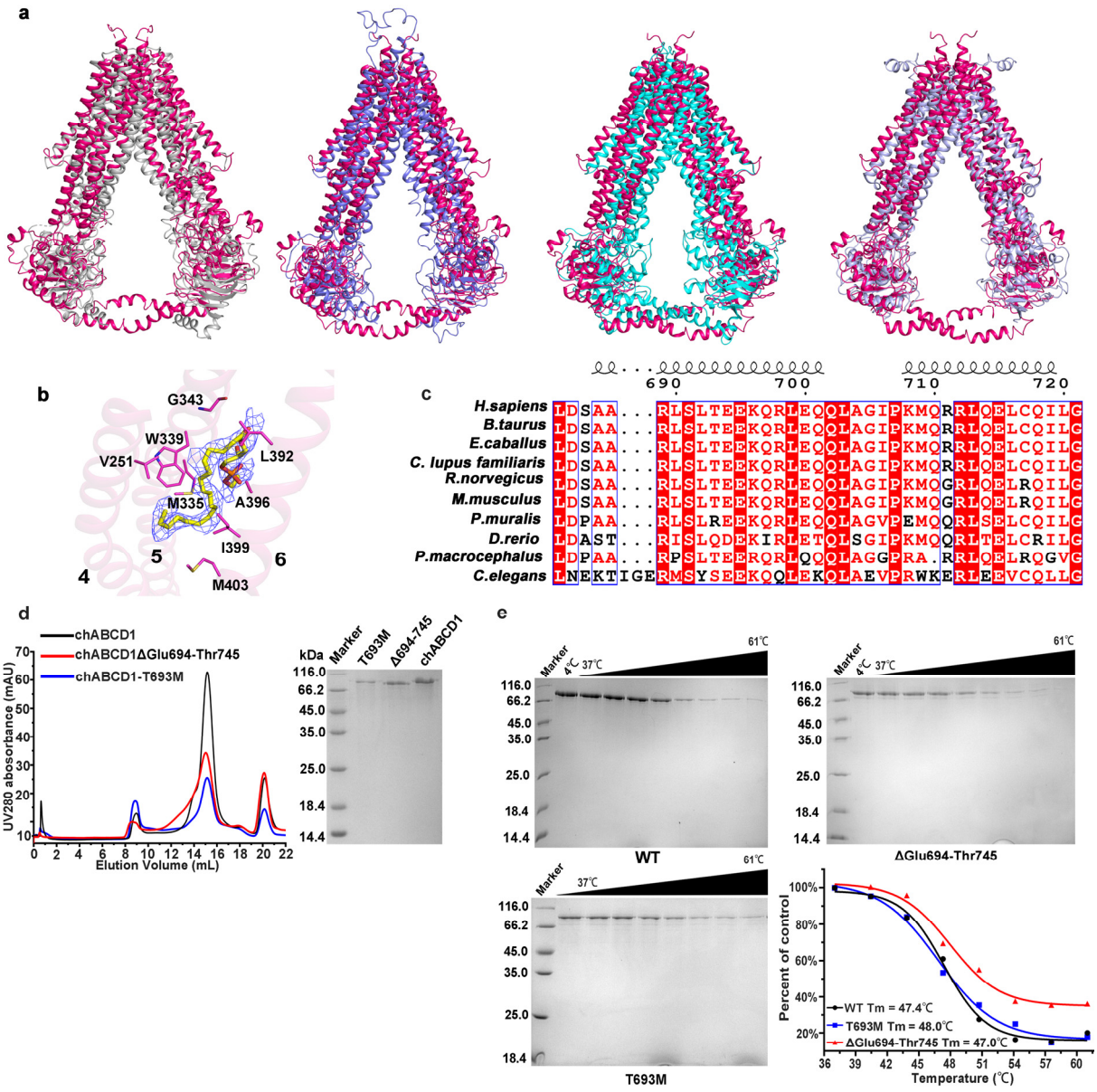


**Supplementary Fig. 5 Structural and biochemical characterizations of the apo-form ABCD1.** **a,** Structural alignment of ABCD1 and the other four type-IV ABC transporters, yielding an RMSD of 9.6, 13.7 10.7 and 26 Å, over 829, 858, 871 and 797 Cα, respectively. Human ABCD1, ABCB6 (PDB ID: 7EKM), ABCB11 (PDB ID: 6LR0), *Saccharomyces cerevisiae* Atm1 (PDB ID: 7SPL) and *Campylobacter jejuni* PglK (PDB ID: 5c76) are colored in rose, gray, marine, cyan and lightblue, respectively. **b,** Density map for a phosphatidyl ethanolamine (PE) molecule**.** A PE

molecule (contour level at 5σ) was inserted into the hydrophobic cleft formed by TM5 and TM6. **c,** Multiple-sequence alignment for the C-terminal helix of ABCD1 and homologs. **d**, The size exclusion chromatography profiles of chABCD1 and mutants of ΔGlu694-Thr745 and T693M using a Superose 6 Increase 10/300 SEC column. The peak fractions around 15mL were applied to SDS-PAGE and visualized by Coomassie-blue staining. The chromatogram and SDS-PAGE are representatives of > 3 independent experiments that showed similar results **e,** The thermal stability assays of chABCD1 and mutants of ΔGlu694-Thr745 and T693M. One time thermal stability assay of chABCD1 and mutants of ΔGlu694-Thr745 and T693M was performed in this project (n=1). Source data are provided as a Source Data file.

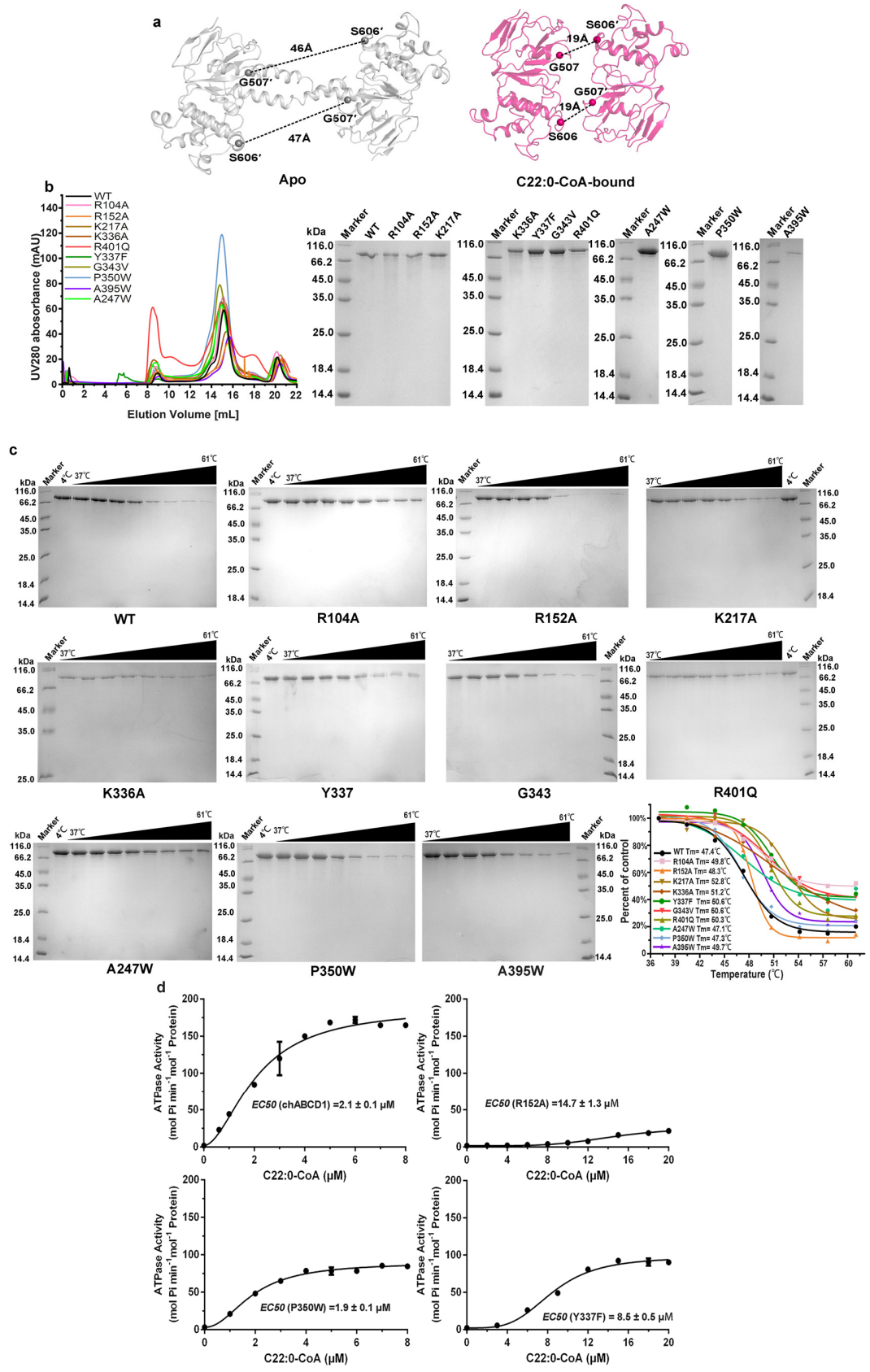
a
S606′
46A
G507′
G507′
47A
S606′
Apo
S606′
19A
G507
G507
19A
S606
C22:0-CoA-bound
b
WT
R104A
R152A
K217A
K336A
R401Q
Y337F
G343V
P350W
A395W
A247W
UV280 abosorbance (mAU)
Elution Volume [mL]
kDa
Marker
WT
R104A
R152A
K217A
K336A
Y337F
G343V
R401Q
A247W
P350W
A395W
c
WT
R104A
R152A
K217A
K336A
Y337
G343
R401Q
A247W
P350W
A395W
Percent of control
Temperature (℃)
WT Tm= 47.4℃
R104A Tm= 49.8℃
R152A Tm= 48.3℃
K217A Tm= 52.8℃
K336A Tm= 51.2℃
Y337F Tm= 60.6℃
G343V Tm= 60.6℃
R401Q Tm= 60.3℃
A247W Tm= 47.1℃
P350W Tm= 47.3℃
A395W Tm= 49.7℃
d
ATPase Activity
(mol Pi min-1mol-1 Protein)
EC50 (chABCD1) =2.1 ± 0.1 μM
C22:0-CoA (μM)
EC50 (R152A) =14.7 ± 1.3 μM
C22:0-CoA (μM)
EC50 (P350W) =1.9 ± 0.1 μM
C22:0-CoA (μM)
EC50 (Y337F) = 8.5 ± 0.5 μM
C22:0-CoA (μM)

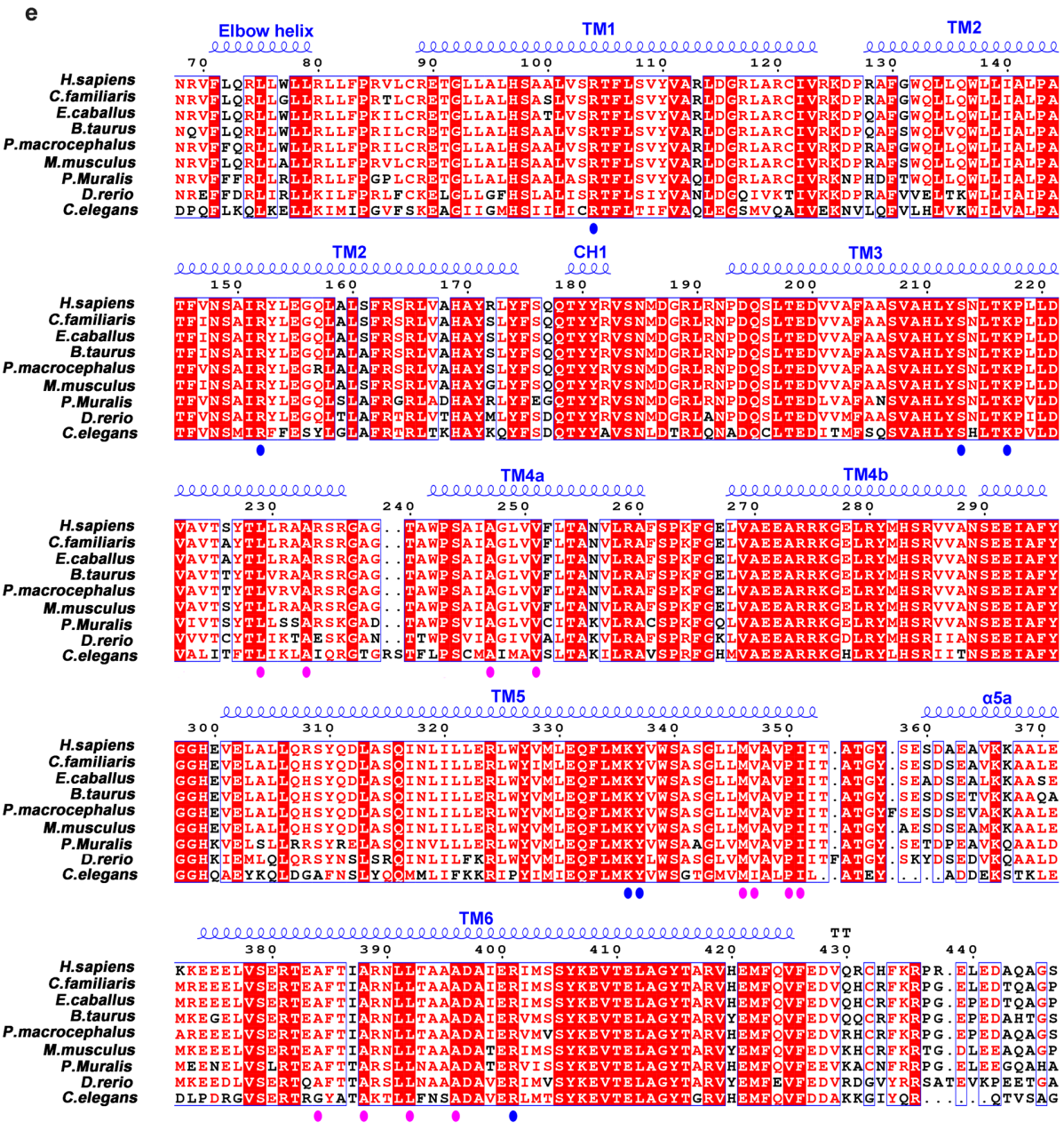


78

79 **Supplementary Fig. 6 Conformational changes of ABCD1 upon substrate binding. a,** The

80 NBDs in apo-form and C22:0-CoA-bound ABCD1, viewed from the peroxisome matrix. The Cα

81 distances between the Walker A and the signature motif are indicated. **b**, The size exclusion

82 chromatography profiles of chABCD1 and mutants related to substrate binding using a Superose

83 6 Increase 10/300 GL SEC column. The peak fractions around 15 mL were applied to SDS-PAGE

and visualized by Coomassie-blue staining. The chromatogram and SDS-PAGE are representatives of > 3 independent experiments that showed similar results. **c,** The thermal stability assays of chABCD1 and mutants related to substrate binding. One time thermal stability assays of chABCD1 and mutants was performed in this project (n=1). Source data are provided as a Source Data file. **d,** Substrate concentration-dependent ATPase activity of chABCD1 and mutants R152A, Y337F and P350W in detergent of LMNG+CHS, upon addition of C22:0-CoA. The data points were fitted with a Hill equation, based on which $EC_{50}$ were calculated. All data points represent means of three independent measurements (n=3). Error bars indicate standard deviation. Source data are provided as a Source Data file. **e,** Multiple-sequence alignment of ABCD1 and homologs. Circles below the alignment indicate residues interacting with the CoA portion (blue) or the fatty acyl chain (pink) portion of the substrate.

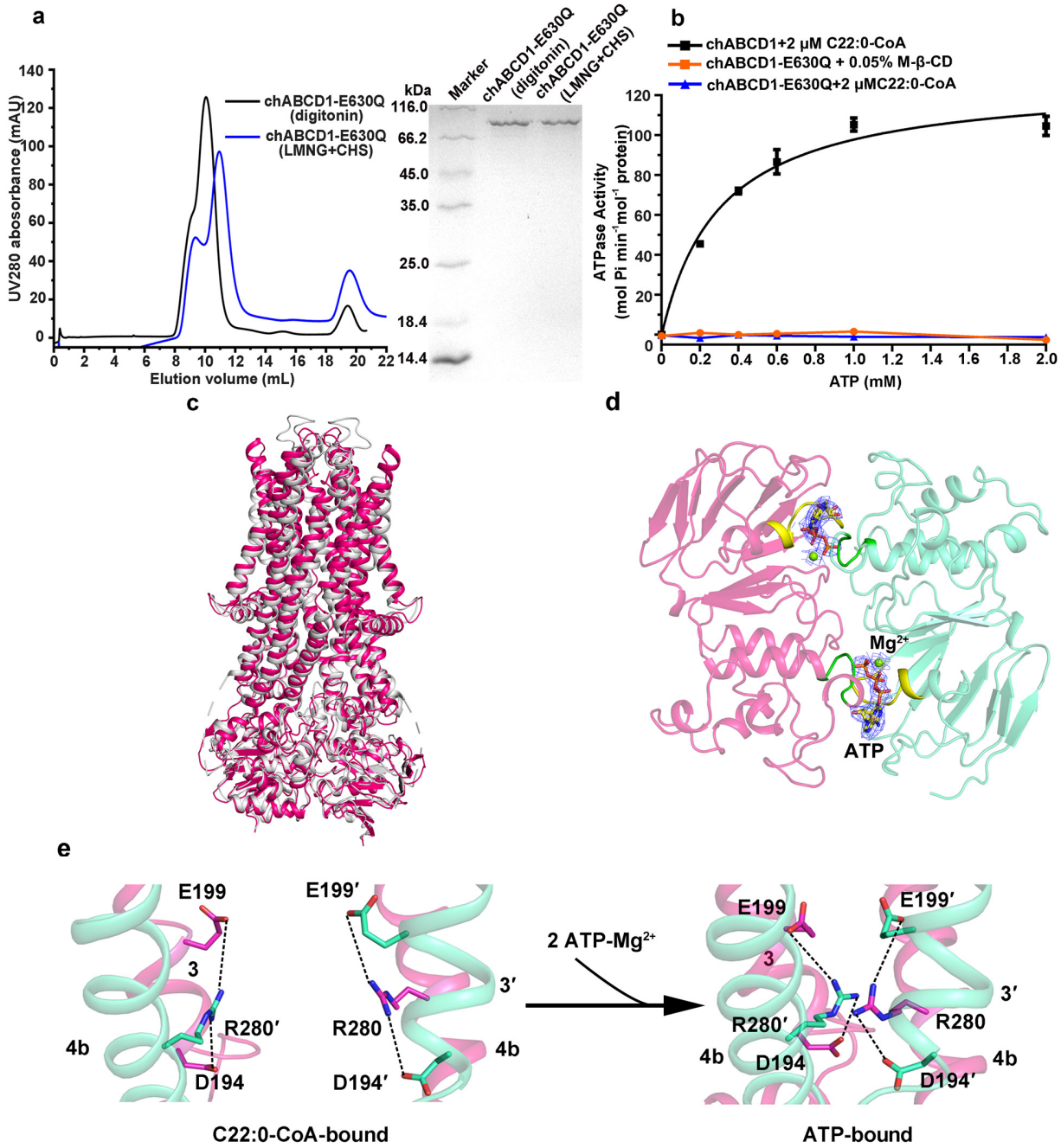


**Supplementary Fig. 7 The structural characterization of ATP-bound ABCD1. a,** The size exclusion chromatography profiles of chABCD1-E630Q in detergent of digitonin and LMNG+CHS with a Superdex 200 10/300 GL SEC column. The peak fractions were applied to SDS-PAGE and visualized by Coomassie-blue staining. The chromatogram and SDS-PAGE are

representatives of 3 independent experiments that showed similar results. **b,** ATPase activities of chABCD1-E630Q in LMNG+CHS in the presence or absence of C22:0-CoA. 0.05% M-β-CD was also tested as the control group. The data points were fitted with a Michaelis-Menten equation. All data points represent means of three independent measurements (n=3). Error bars indicate standard deviation. Source data are provided as a Source Data file. **c,** Superposition of ATP-bound ABCD1 (rose) and ATP-bound ABCD4 (PDB ID:6jbj, gray). **d,** The density maps for ATP-$Mg^{2+}$ molecules are contoured at 5σ. ATP molecules are shown as yellow sticks; $Mg^{2+}$ ions are displayed as green spheres. Walker A and signature motif are colored in yellow and green, respectively. **e,** The TM3/TM3′ and TM4b/TM4b′ in C22:0-CoA- and ATP-bound ABCD1 are shown in cartoon, respectively. The residues at the cytosolic gate are shown as sticks and salt bridges are shown as dotted lines.

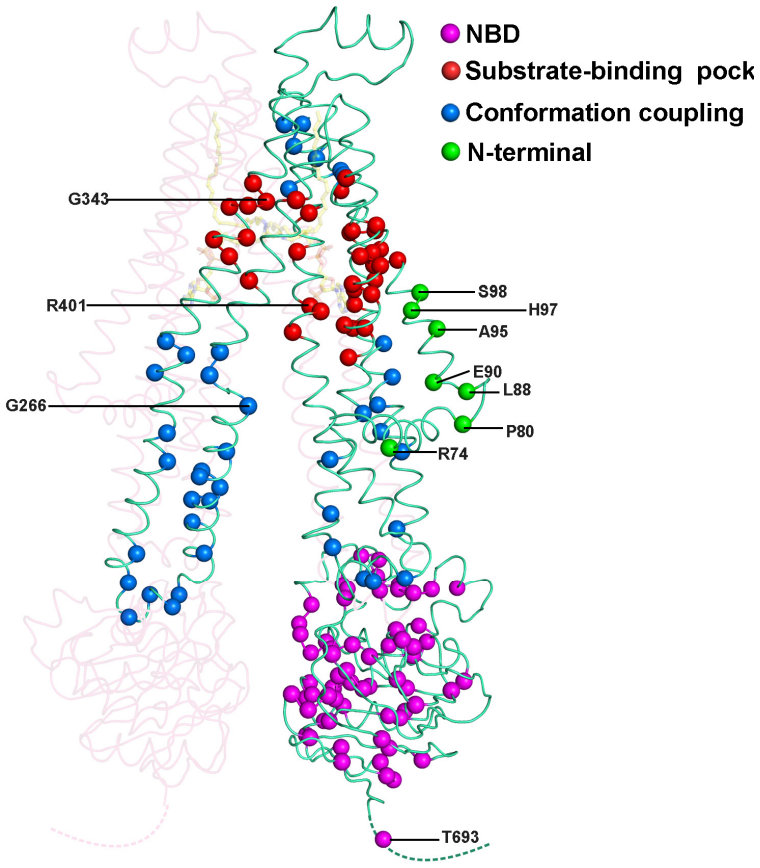


**Supplementary Fig. 8 Distribution of X-ALD associated pathogenic variants in ABCD1.** The four groups of mutant residues are represented as dots in different colors. The unfolded C-terminus of ABCD1 are shown as dotted line. The pathogenic variants discussed in this manuscript are labelled.

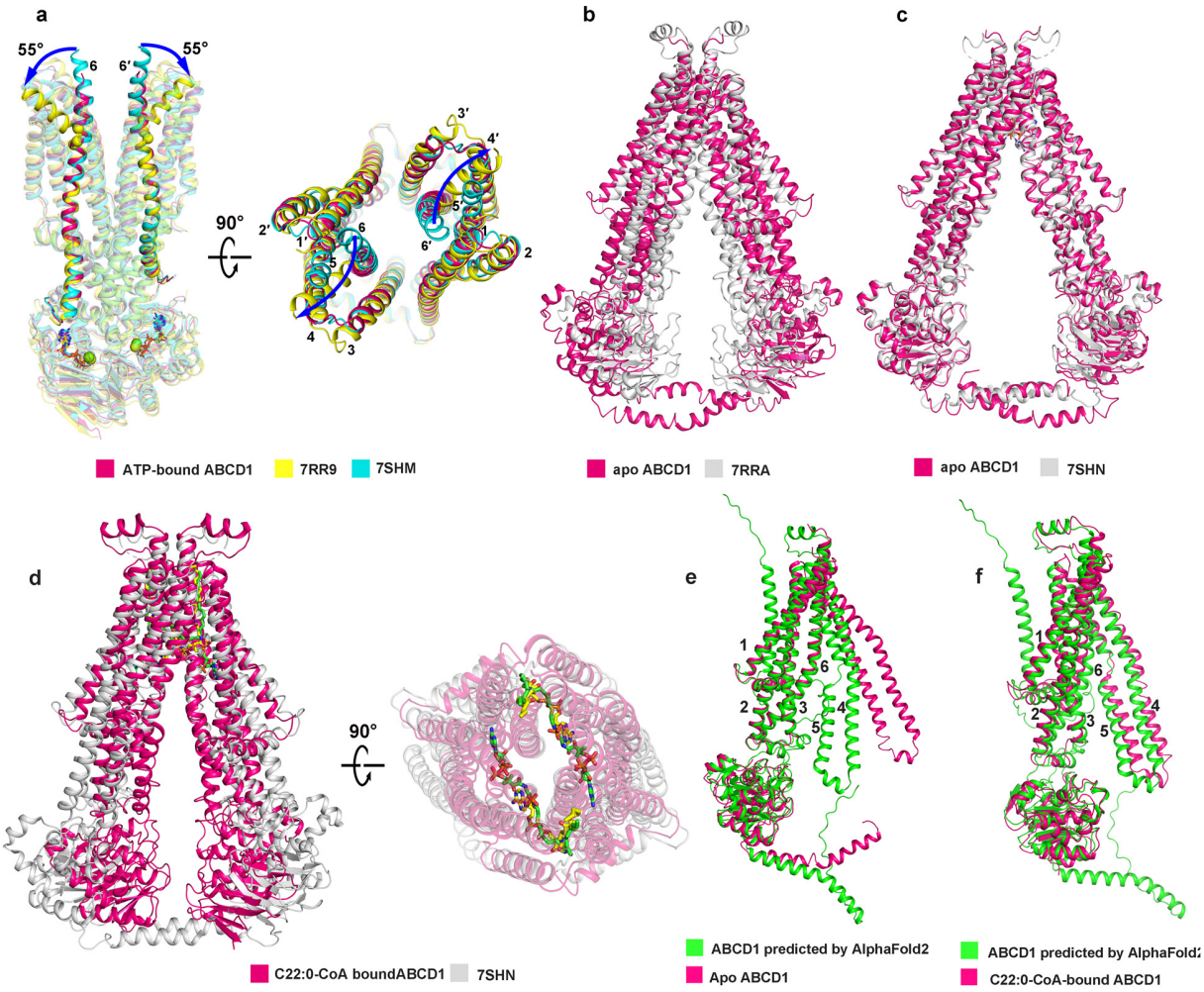


**Supplementary Fig. 9 Structural superpositions of our ABCD1 structures against the recently reported ABCD1 structures (labelled with corresponding PDB codes). a,** Structural superposition of reported ATP-bound ABCD1 structures. **b** and **c**, Structural superposition of our apo-form ABCD1 structure with the other reported apo-from structures respectively. **d**, Structural superposition of our apo-form structure with the oleyl-CoA-bound structure. The oleyl-CoA and C22:0-CoA are shown as yellow and green sticks, respectively. **e** and **f**, Structural superposition of our apo-form ABCD1 protomers with predicated ABCD1 protomer by AlphaFold2. Protomers form apo-form ABCD1 and C22:0-CoA-bound ABCD1 are superposed with the predicated protomer, respectively.

**Supplementary Table 1 Cryo-EM data collection, refinement and validation statistics.**

| | Apo ABCD1 (EMDB-32152) (PDB 7VWC) | C22:0-CoA-bound ABCD1 (EMDB-32224) (PDB 7VZB ) | ATP-bound ABCD1 (EMDB-32171) (PDB 7VX8 ) |
|---|---|---|---|
| **Data collection and processing** | | | |
| Magnification | 22,500 | 22,500 | 81,000 |
| Voltage (kV) | 300 | 300 | 300 |
| Electron exposure (e–/Å2) | 60 | 60 | 54 |
| Defocus range (μm) | -2.0 to -1.5 | -2.0 to -1.5 | -2.0 to -1.8 |
| Pixel size (Å) | 1.07 | 1.07 | 1.07 |
| Symmetry imposed | C1 | C2 | C2 |
| Initial particle images (no.) | 4,094,944 | 6,943,977 | 1,878,754 |
| Final particle images (no.) | 360,311 | 336,741 | 550,864 |
| Map resolution (Å) | 3.5 | 3.6 | 2.8 |
| FSC threshold | 0.143 | 0.143 | 0.143 |
| Map resolution range (Å) | 2.9-4.1 | 2.9-4.1 | 2.2-3.0 |
| | | | |
| **Refinement** | | | |
| Initial model used (PDB code) | *ab initio* | *ab initio* | 6jbj |
| Model resolution (Å) | 3.5 | 3.6 | 2.8 |
| FSC threshold | 0.143 | 0.143 | 0.143 |
| Map sharpening B factor ($Å^2$) | -117.5 | -185.8 | -116.8 |
| Model composition | | | |
| Non-hydrogen atoms | 9,854 | 9,463 | 9,018 |
| Protein residues | 1,223 | 1,172 | 1,120 |
| Ligands | Two PE molecules | Two CHS and Two C22:0-CoA molecules | Two ATP molecules and Two $Mg^{2+}$ |
| *B* factors ($Å^2$) | | | |
| Protein | 61.77 | 89.73 | 39.77 |
| Ligand | 51.01 | 57.83 | 28.26 |
| R.m.s. deviations | | | |
| Bond lengths (Å) | 0.010 | 0.009 | 0.009 |
| Bond angles (°) | 0.975 | 0.889 | 0.992 |
| Validation | | | |
| MolProbity score | 2.06 | 2.10 | 1.77 |
| Clashscore | 10.52 | 14.43 | 7.41 |
| Poor rotamers (%) | 0.38 | 0.00 | 1.06 |
| Ramachandran plot | | | |
| Favored (%) | 91.13 | 91.91 | 95.13 |
| Allowed (%) | 8.87 | 8.09 | 4.87 |
| Disallowed (%) | 0.00 | 0.00 | 0.00 |

**Supplementary Table 2 The X-ALD associated pathogenic variants in ABCD1.** Four groups of X-ALD associated pathogenic variants in ABCD1 are listed, which are displayed in Supplementary Fig. 8. The residues in the NBD, substrate-binding pocket, conformation coupling and N-terminal are colored in magenta, red, blue and green, respectively, the same color as those in the Supplementary Fig. 8.

| | | |
|---|---|---|
| P484D | S633R | R113C, R113P |
| L493P | V635M | L114P |
| M501L | S636I | G116R, G116D, G116E |
| L503P, L503M | D638Y | A119D |
| G507S, G507D | E640K | R120P |
| N509I (Walker A motif, ATP-binding residue) | A646P | L154P |
| G510S, G510D (Walker A motif, ATP-binding residue) | L654P | L158P |
| C511Y (Walker A motif, ATP-binding residue) | L655P | L160P |
| G512S,G512D (Walker A motif, ATP-binding residue) | T658I | R163C, Arg163H, Arg163L, Arg163P |
| K513Q, K513R (Walker A motif, ATP-binding residue) | R660W, R660Q, R660P | L166P |
| S514R, S514G, S514I, S514N (Walker A motif, $Mg^{2+}$-binding residue) | L663Q | Y174D, Y174S |
| S515F (Walker A motif, $Mg^{2+}$-binding residue) | H667D, H667L | Q178E |
| L516P | T668P, T668I | Y181C |
| R518G, R518Y,R518Q (ATP-binding residue) | H669Y, H669R | R182P |
| L520P | W679R, | R189W |
| G522R | T693M | D194N, D194H |
| L523F | S103R | E199K |
| P525S | R104C, R104H | D200N |
| G529S, G529D | T105P, T105I, | A205E |
| K533E, K533N | T107P | S262W |
| P534S, P534L, P534R | S108L, S108W | P263L |
| F540 | W137S | G266R, G266E |
| P543S, P543L | A141T | A273E |
| Q544K,Q544R (Q-loop, $Mg^{2+}$ and ATP-binding residue) | P143A, P143S, P143H, P143L | R275W |
| Y547C | V147G | K276E |
| M548V | N148D, N148Y, N148S | G277R, G277W |
| S552P | S149N, S149R | L279P |
| R554H | R152S, R152P | R280C, R280L |
| Q556R | L211P | H283Y, H283D, H283R |
| Y559C | S213C | R285G, R285P |
| P560L, P560R | N214D | E291K, E291G, E291D |
| D561V, | K217E | E292K |
| M566K, M566K, M556T | P218S | A294T, |
| L576P | L220P | Y296C |
| R591Y, R591L, R591P, R591Q (ATP-binding residue) | D221G | G298S, G298D |
| G594R | V224G | E302K, E302Q, |
| A597G | L229P | L313P |
| L605Q | A245D | Q316P |
| S606P, S606A, S606L (Signature motif, ATP-binding residue) | T254A,254P, T254M | L322P |
| G607D (Signature motif, ATP-binding residue) | K336M, K336N | R324C |
| G608S (Signature motif, ATP-binding residue) | Y337H | L325P |
| E609K, E609G (Signature motif, ATP-binding residue) | W339R, W339S | T382P |
| A616T, A616V | A341D | R389G |
| R617S, R617D, R617G, R617S, R617G, R617C, R617H | S342P | R74W |
| Y620H, Y620C | G343S, G343V | P84L |
| A626T | L344P | C88W |
| L628P | L392V | E90K |
| D629N, D629H | A396T | A95D |
| E630K (Walker B motif, ATP-binding residue) | R401W, R401G, R401Q | H97P, H97L |
| C631R,C631Y,C630W | I402N | S98P, S98L, S98W |
| T632P, T632I | S404P | |